Angular modeling of a rotating machine: Application to study the dynamic behavior of an electric powertrain in non-stationary conditions

Steve Koshy Mathew, Adeline Bourdon, Didier Rémond

Angular modeling of a rotating machine: Application to study the dynamic behavior of an electric powertrain in non-stationary conditions

S.K. Mathew, A. Bourdon, D. Remond
University of Lyon, LaMCoS, INSA Lyon, CNRS,
UMR5259, 69621 Villeurbanne, France
e-mail: **steve-koshy.mathew@insa-lyon.fr**

Abstract
Electric engines are now moving in the direction of higher speed and larger torque to achieve higher performance. Therefore, predicting accurately the non-stationary loads and deformations during these regimes is of utmost importance. This paper aims to describe the first steps to a simplified coupled model of the electric powertrain to evaluate its dynamic behavior under non-stationary conditions considering the gyroscopic effects. The developed numerical model is based on the angular approach, which introduces explicitly the machine's free body rotation degrees of freedom, which is different from the classical approaches, where speed is generally considered constant. Integration of a simplistic novel bearing model is done to demonstrate the effects of the excitations due to the rolling element-races interactions on the dynamic behavior of the system under non-stationary conditions. The expected results will provide a base model which can be used for phenomenological analyses, for complex models of bearings, gears, and motors.

1 Introduction

Electric Mobility has grown its importance in the industry specifically in automotive, from the inclusion of environmental and energy regulations laid out in the United Nations Climate Change Conference held in Paris in 2015 [1]. The emergence of electric and hybrid vehicles has also triggered the adherence to more stringent NVH attributes. The NVH characteristics of an electric powertrain are an essential factor during the design of the system because of its contribution to overall cabin noise during acceleration and deceleration. The experimental prediction of NVH characteristics of the complex drivetrain is expensive and time-consuming and it also gives very limited access to play with the design attributes of the entire assembly. Computer simulation technology is becoming more widely used because it has progressed to the point where it can provide detailed information to designers for this multi-physics phenomenon connected to the system.

Rotating components such as an electric powertrain have many components (electrical motor, gears, bearings, timing belts, etc.) that are sources of periodic excitations during their operation due to their discrete periodic geometry. These can be efficiently described in the multi-physics modeling. These excitations are interactions through various structural components which are in rotation or rest (shaft, housing, etc.). There have been a lot of recent numerical simulation attempts to simulate different elements in the drivetrain e.g. a motor or a gear train for NVH studies. [2] developed a simulation model to study the acoustic radiation of a switched reluctance motor of the electrical machine using finite element methods. [3] developed a multi-physics simulation environment which was used to estimate the radial forces of a permanent magnet synchronous machine for light traction, He also used this model to do sound pressure evaluation for different operating conditions. [4] developed a statistical model for gears noise prediction in gearbox applications. [5] studied the effects of transmission error and bearing preload on gearbox noise. While these studies and models help us understand the physical attributes of various phenomena occurring in each element of a drivetrain, it fails to capture the combined effects of elements in the system and their coupling with the global rotation

of the machine. Few studies have tried to integrate different connecting elements of a powertrain such as a motor and gear-train and performed structural simulation on the gearbox housing due to the excitations from motor and gear-train using FEA [6], [7] and [8]. However, most of the models in the literature are built under the assumption that the rotating speed is constant. The dynamics of connecting elements of a rotating machine cause excitations that occur recursively and are inherently periodic and these excitations are inherently dependent on the rotation speed even if the machine is under a stationary regime. For E.g. in the case of bearing rotor systems, roller-races interactions produce fluctuation in the forces due to the bearing which is dependent on the shaft rotation speed [9]. So, it is of utmost importance that speed needs to be considered as an implicit variable of the simulation rather than a defined parameter.

Time-based modeling follows the traditional approach, in which, all the variables are measured and analyzed w.r.t time depending upon the application. The classical approach to dealing with multi-source dynamic excitation in the rotating machine is to use time-dependent solvers. But it should be noted that many of these excitation sources are generally dependent on time and also the angle of rotation. When we consider the dynamic behavior of an electric motor, Torque characteristics are a function of both the current excitation which is dependent on time and waveform, and the permanent magnetic field attributes which are dependent on the angle of rotation of the rotor [10]. Time-based solvers sometimes fail to track these excitations prevalent in the system [11]. Modeling the system in the angular domain, in which motion equations are translated into the angular domain stresses the need to know precisely the relationship between time and angular position of the rotating part [12]. Time becomes an explicit variable of the angular position. This modeling technique is very useful when analyzing rotating components with discrete periodic geometries that generate different cyclic excitations. Using the angular domain approach, we can establish a strong coupling between the rotating speed and the dynamics of the system. This is predominantly more evident when working with high-speed rotors and where gyroscopic effects are introduced [13, 14, 15]. By introducing this academic model, the main purpose is to show that suppressing constant speed assumption may change the model classically used in the literature.

The primary focus of using the angular approach is to study the effects of the integration of discrete periodic connecting elements such as bearing, gear, and e-motor that invokes the effects of all the components' geometry provoking interactions forces leading to perturbations of the angular speed. In this paper, bearings have been modeled and a harmonic excitation has been introduced to show these interactions and coupling effects on the system. The model introduces the angular modeling approach to explain how the system response varies at different operating conditions due to the torque variations induced into the shaft by the bearing dynamics.

Rotating shafts have been used in almost all industrial machines such as steam and gas turbines, turbo generators, and ICE. Therefore, it is necessary to investigate the behavior of these systems under various operating conditions, particularly when there are vibrations on the bearing supports, which has to be resilient to critical speeds or torque or force fluctuations caused by gyroscopic movements because damages to the bearing can cause catastrophic failures. There have been numerous studies on the dynamic response of geared rotor-bearing systems. Some of them were based on the experimental response of the bearing while others were based on theoretical analysis of mechanical component failures. Sawalhi and R.B. Randall [16], developed a simulation model for a gearbox test rig for bearing localized faults, which relates the raceway displacement to the bearing load and also accounts for the slippage between the elements, which incorporates Hertzian contact theory. This model is very useful when localized bearing faults are considered as it considers the slippage in the bearing and also the non-linearity in bearing stiffness but it had the limitation of assuming speed as constant. Another example of a numerical approach to bearing modeling, Singh [17], developed a dynamic nonlinear model of the rolling element with an outer raceway line spall. The modeling approach involved modeling all the components of the bearing (outer and inner rings, rolling elements, and cage) as flexible bodies which predicts the impulsive contact forces that generate bearing vibrations. These approaches are suitable to produce simulated signals that can emulate very specific fault behavior but they do not allow to describe the dynamic variation of magnitude in forces and torques that occur in bearings due to speed fluctuations, even in stationary regimes. However, these complex bearing models are extremely difficult to integrate into global architectures due to high computational cost, and also our initial aim is to study the behavior of these systems irrespective of their faults in the global setup.

So, when analyzing NVH for complex architectures with multiple components, the state-of-the-art approach uses coupled finite element (FE) analysis in a generalist multi-physics package. These are time-consuming and solving computationally intensive. Another approach is to combine numerical and analytical models, but complex numerical models for each component (for example a bearing) as described in the above literature study are not feasible as they are computationally intensive. So in many complex architectures, the modeling approaches neglect the modeling of bearing since the excitation caused by the bearing is inferior compared to other significant parts in the driveline. In the multiphysics model developed by [8], to evaluate the NVH performance of an electric powertrain, the bearings were considered as a revolute joint connected to the housing. Another approach shown by [18], introduces a global dynamic model to study responses of drivetrains under different excitations such as the dynamic mesh force acting at the gear teeth, dynamic loads acting at the bearings, and motor torque fluctuation excitation. In this approach, the bearing is modeled as a stiffness matrix calculated at static conditions. One approach to solve this issue is by considering the bearing as restitution forces that are dependent on the rotating speed of the shaft which is explored in the model. These limitations have been incorporated in our modeling approach, where the bearings have been modeled using a simplistic model yet having strong coupling considering the rotation of the shaft. The bearing modeling approach presented in the next section is based on the rolling resistance phenomena based on the interaction between the races and the rolling elements [19]. This approach has been used for normal force and resistive torque estimation. This choice was made to assure the possibility of coupling the model into more complex mechanical architectures. From the literature, it is evident that most of the models are based on the constant speed of the rotating shaft. The novelties of our model include the use of the angular approach, which is built considering no assumption on the IAS to study the effects of interactions and couplings of the connecting elements in a simple power train architecture and show the impact of the assumptions traditionally made on NVH models especially working under non-stationary conditions.

The general description of the powertrain model, described above is presented in Section 2. Section 2.2 discusses the Euler angle transformation technique used in this model. Section 2.3 discusses the bearing model, which includes the introduction to the rolling resistance phenomenon. Section 2.4 discusses the gear model used in this architecture. Section 2.5 presents the equation of motion and the overall dynamic equation of the system. The results from this model are presented in Sections 3 and 4.

2 Modelization of electric powertrain model

2.1 General Model description

The first application could be extracted from a generalized architecture of an electric drive-train including a gear reducer.

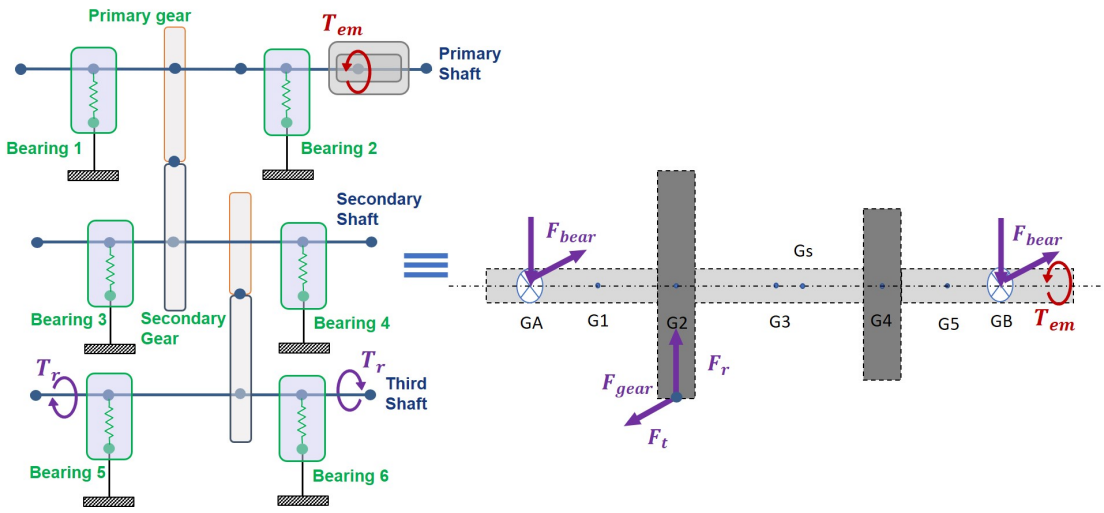

Figure 1: Rotor Bearing Model

The dynamic model considered for this analysis is a reducer of standard automotive e-powertrain as shown in Figure 1. This reducer academic model is made of a rigid shaft, rigid disk, and bearings with constant stiffness which will be explained in the following sections (Figure 1). Bearing excitation is due to the fact that the number of rolling elements under load is fluctuating and it has been introduced into the system as a cyclic excitation. The gears are asymmetric to the shaft center. We assume that torque is induced by the rotating equipment, and we make no preliminary assumptions about the rotational speed. The resistive forces are assumed to be acting on one of the gears which cause displacements at the bearing center that can be extracted as bearing forces. An analysis of the impact of the different assumptions on the equations of motion of each component of the rotor is explored.

2.2 Transformation of referential axis and rotation vector

We define R_0 ($\vec{X}$,$\vec{Y}$,$\vec{Z}$) as the fixed coordinate system or inertial frame referenced in the Galilean reference. R ($\vec{\tilde{x}}$,$\vec{\tilde{y}}$,$\vec{\tilde{z}}$) the rotating coordinate system referenced in the local reference after the movement of the shaft element due to its rotations and translations, and it coincides with the main axis of the cross-section of the shaft. The motion of the rotating shaft, in three-dimensional motion, can be completely described using Euler's angles defined via three successive rotations to specify the relations between the principal axes of the rotating frame ($\vec{\tilde{x}}$,$\vec{\tilde{y}}$,$\vec{\tilde{z}}$) and the fixed frame ($\vec{X}$,$\vec{Y}$,$\vec{Z}$) as shown in Figure 2.

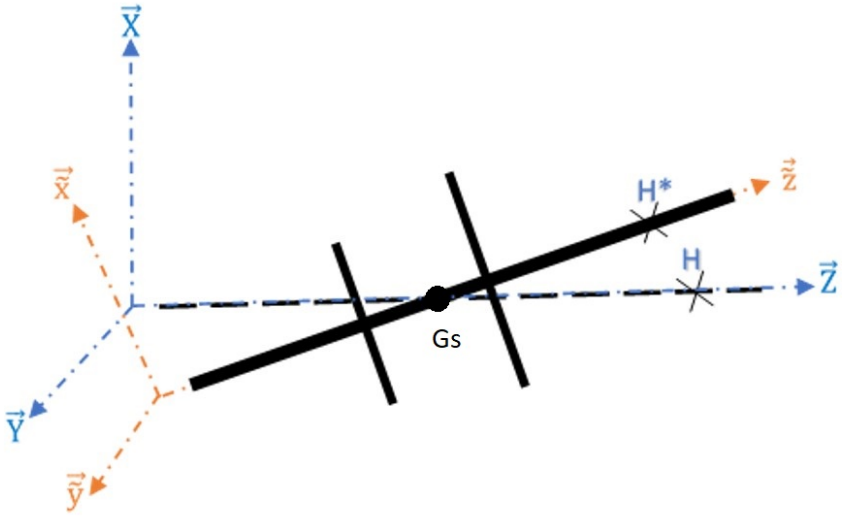

Figure 2: Illustration of the different frames

H is any point coinciding on the main axis of the rotor shaft and Gs is the center of gravity of the system. H* is the same point on the shaft after the displacements. The movement of the shaft is described by a rotation sequence, appealing to Euler angles.

The orientation of the elements of the model in the inertial frame can then be described using one transformation matrix $[P_R^{R_0}]$ given by:

$$[P_R^{R_0}] = \begin{bmatrix} cos(\varphi_y) & sin(\varphi_x).sin(\varphi_y) & -cos(\varphi_x).sin(\varphi_y) \\ 0 & cos(\varphi_x) & sin(\varphi_x) \\ sin(\varphi_y) & -sin(\varphi_x).cos(\varphi_y) & cos(\varphi_x).cos(\varphi_y) \end{bmatrix} \tag{1}$$

$$[P_{R_0}^R] = \begin{bmatrix} cos(\varphi_y) & sin(\varphi_x).sin(\varphi_y) & cos(\varphi_x).sin(\varphi_y) \\ 0 & cos(\varphi_x) & -sin(\varphi_x) \\ -sin(\varphi_y) & sin(\varphi_x).cos(\varphi_y) & cos(\varphi_x).cos(\varphi_y) \end{bmatrix} \tag{2}$$

Using the transformation matrix $[P_R^{R_0}]$, The angular velocity and its corresponding components can be expressed in the direction of the principal axis as :

$$\vec{\omega}(R/R_0) = \dot{\varphi_x}\vec{X} + \dot{\varphi_y}\vec{y_1} + \dot{\theta}\vec{z_2} \tag{3}$$

$$\omega_x = \dot{\varphi_x}\cos\varphi_y\cos\theta + \dot{\varphi_y}\sin\theta \tag{4}$$

$$\omega_y = -\dot{\varphi}_x\cos\varphi_y\sin\theta + \dot{\varphi_y}\cos\theta \tag{5}$$

$$\omega_z = \dot{\theta} + \dot{\varphi_x}\sin\varphi_y \tag{6}$$

2.3 Excitations

2.3.1 Bearing model (With no abnormal excitations)

The fundamental components of a rolling element ball bearing are the outer race (OR), the inner race (IR), the cage, and the rolling elements (which in our case are balls). Using Hertz's theory, the forces characterizing the dynamic interactions between the shafts and the supports are described as a function of the IR and OR displacements. The estimation of bearing forces introduced in the model, as demonstrated in this section, is appropriate for non-stationary input torques. The analysis that follows is based on the following assumptions:

1. There is no slippage between the Outer Race (OR), the Inner Race (IR), and the rolling elements.
2. The rolling elements are in quasi-static equilibrium, meaning that the normal contact force between the IR and a given rolling element is equal to the normal force between the OR and the mentioned rolling element. We also neglected the associated centrifugal force due to rotation.
3. Surface imperfections that led to localized defects are neglected in the current model.

The modeling approach is based on the hypothesis that the rolling resistance phenomenon occurs due to the interaction between the races and the rolling elements developed by [19]. The displacement of the normal force introduces a tangential force which is introduced in the equation (7) and this force is translated as torque as opposed to the direction of the angular speed of the rolling element. This torque may be associated with the frictional moment and in consequence, the rolling resistance coefficient is considered by the analogy of the constant friction coefficient.

$$F_t = \mu.F_r \tag{7}$$

2.3.2 Bearing forces and frictional torque

The bearing characteristics needed for the model description are: the number of rolling elements Z, the rolling element radius r, the rolling element mass m and inertia I, the inner and outer contact diameter of the rolling element with the races (Di and De), the defect frequency of the outer race BPFO, contact angle of the ball and race α and the ball diameter D.

The nominal ball-raceway normal load F_r as a function of deflection δ, which is the displacement at the bearing center and is defined as :

$$F_r = K.\delta \tag{8}$$

where is K stiffness of the bearing in X and Y direction.
The displacements at the center of gravity of the system are defined in translation as $\overrightarrow{d}$ and rotation is $\overrightarrow{r}$, where $\overrightarrow{d}$ and $\overrightarrow{r}$ are given by :

$$[\overrightarrow{d}] = \begin{bmatrix} u \\ v \\ w \end{bmatrix} ; [\overrightarrow{r}] = \begin{bmatrix} \varphi_x \\ \varphi_y \\ \theta_z \end{bmatrix} \tag{9}$$

Since the shaft is rigid, we can estimate the displacements in the center of the inner ring of bearing as,

$$\overrightarrow{d_{bear}} = [\overrightarrow{d}] + \overrightarrow{G_s G_i} \wedge [\overrightarrow{r}] \tag{10}$$

where $\overrightarrow{G_s G_i}$ is the distance between the center of gravity of the system (G_s) to the center of each bearing (G_i), which is given by,

$$\overrightarrow{G_s G_i} = \begin{bmatrix} 0 \\ 0 \\ Z_i \end{bmatrix} \tag{11}$$

where Z_i is the distance from the center of gravity of the system (G_s) to the center of each bearing (G_i) in $\vec{Z}$ axis. The δ used in the equation (8) is given by

$$\delta = |\overrightarrow{d_{bear}}|; \overrightarrow{n} = \frac{\overrightarrow{d_{bear}}}{\delta} \tag{12}$$

where $\overrightarrow{n}$ is the direction of the displacement, and the overall force acting on the bearing is given by :

$$F_{bear} = (F_r + \Delta F_r).\overrightarrow{n} \tag{13}$$

It is to be noted that the estimation of the bearing forces can be extended to more advanced models with non-linear stiffness based on Palgrem's model [20]. The fluctuations in the bearing loads ΔF_r are due to the fact that the number of rolling elements under load is fluctuating. It is a function of the angular position θ and the BPFO of the bearing which can be represented as:

$$\Delta F_r = a_f . \sin(BPFO.\theta).F_r \tag{14}$$

a_f is a co-relation factor that depends on the machine and is extracted by experimental data co-relation with simulation results [19].

The nominal frictional torque is also calculated, considering the rolling resistance phenomenon explained in the above section, from the bearing forces, which is given by :

$$T_f = F_t.\frac{Di}{2} = \frac{1}{2}.\mu.Di.Fr \tag{15}$$

Since T_f is related to F_r, ΔT_f can be written in the same way ΔF_r as:

$$\Delta T_f = a_{cf} . \sin(BPFO.\theta).T_f \tag{16}$$

2.4 Gear model

The following modeling strategy is based on a very traditional approach that has been widely used in the literature. Gears are generally regarded as rigid cylinders linked by restorative forces, with paired gear

stiffness representing the contribution of the ensemble of deformable parts. Though in our case, we consider just one shaft and effort acting on the primary gear is introduced as an equivalent load. The main parameters of the gears used in the approach are the pressure angle α and the pitch radius R_p.

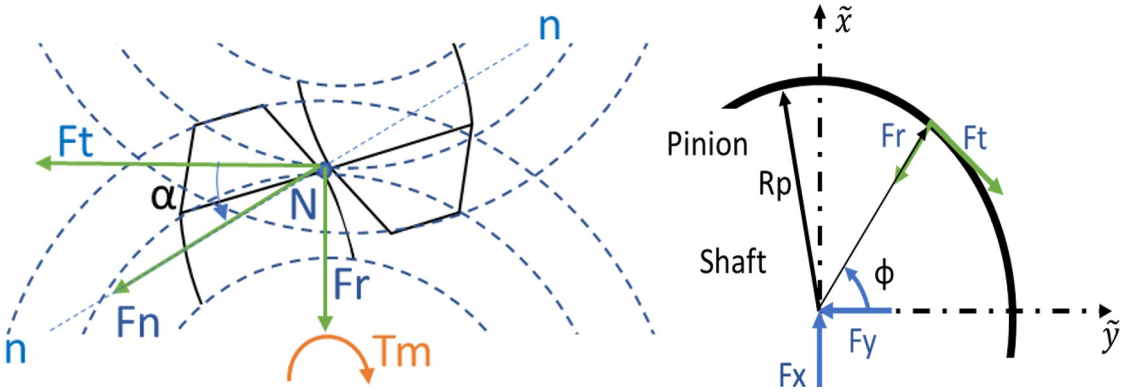

Figure 3: Gear simple model

We assume that only one pair of teeth are in contact during meshing. Gear tooth 1 transmits motion, which stresses gear tooth 2 which takes motion as shown in Figure 3. The loads are applied on the contact point of the gears, which is on the gear pitch at point N. The transversal load F_n is resolved giving radial component F_r and tangential component F_t. The moment due to motor load torque T_m is directly transmitted to the gear as the tangential components F_t. So The torque T_m acting at gear with a pitch radius R_p, is given by:

$$|F_t| = \frac{|T_m|}{R_p} \tag{17}$$

The radial load F_r is calculated by using the equation:

$$|F_r| = |F_t|.\tan(\alpha) \tag{18}$$

The gear contact is not considered to be exactly lying on the local referential axis as shown in Figure 3, rather it is at a given angle due to the gear position and is defined as ϕ. The X and Y components of the F_r and F_t are resolved w.r.t ϕ to get the load acting on the gear in the local referential axis R ($\vec{\tilde{x}}$,$\vec{\tilde{y}}$,$\vec{\tilde{z}}$), which is given by :

$$\{F_{gear}\}_R = \begin{Bmatrix} |F_t|.\sin(\phi) - |F_r|.\cos(\phi) \\ -|F_t|.\cos(\phi) - |F_r|.\sin(\phi) \\ 0 \end{Bmatrix} \tag{19}$$

The force vector $\{F_{gear}\}$ is then transformed to Galilean referential R_0 ($\vec{X}$,$\vec{Y}$,$\vec{Z}$) by :

$$\{F_{gear}\}_{R0} = [P^R_{R0}].\{F_{gear}\}_R \tag{20}$$

The fact the gear forces are not acting at the center of the gravity of the shaft (G_s) produces the moment at that point due to these forces and is given by,

$$\{M_{gear/Gs}\}_R = \overrightarrow{GsO}_R \wedge \{F_{gear}\}_R \tag{21}$$

where $\overrightarrow{GsO}$ is the distance from the center of gravity of the system to the gear center and is given by:

$$\overrightarrow{GsO}_R = [P_{R0}^R].\begin{Bmatrix} R_p.\cos(\phi) \\ R_p.\sin(\phi) \\ Z_g \end{Bmatrix} \tag{22}$$

The moments and the associated directions are in the local referential axis which are defined by the Euler angles and the choice of the Euler angles as parameters of the model amounts to considering three angles that are not defined around orthogonal axes and which do not correspond to the rotations around the axes of the Galilean, so we need to transform the moments by a rotation sequence used during the initial transformation.

$$(M_{gear/Gs})_{\vec{X}} = \{M_{gear/Gs}\}_R.\begin{Bmatrix} 1 \\ 0 \\ 0 \end{Bmatrix} \tag{23}$$

$$(M_{gear/Gs})_{\vec{y_1}} = \{M_{gear/Gs}\}_R.\begin{Bmatrix} 0 \\ \cos(\varphi_x) \\ \sin(\varphi_x) \end{Bmatrix} \tag{24}$$

$$(M_{gear/Gs})_{\vec{z}} = \{M_{gear/Gs}\}_R.\begin{Bmatrix} \cos(\varphi_x).\sin(\varphi_y) \\ -\sin(\varphi_x) \\ \cos(\varphi_x).\cos(\varphi_y) \end{Bmatrix} \tag{25}$$

2.5 Equation of motion

The mathematical model for the dynamic behavior of the rotor is developed by extracting the kinetic and potential energy of different components of the rotor.

2.5.1 Shaft and disk

The shaft, gears, and bearings are discretized into several parts with each considered as a separate element with mass (mi) and center of mass (Gi) as shown in Figure 4.

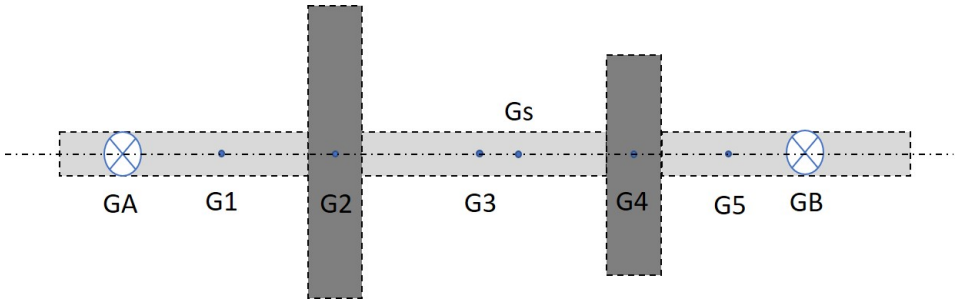

Figure 4: Rotor Representation

The overall equation of motion is w.r.t the center of gravity of the system (Gs). The disks and the shaft are assumed to be rigid. The kinetic energy (both translational and rotational) is derived relative to the displacement of the system at its mass center Gs (u, v, w) written in the rotating frame using the Euler angles (φ_x, φ_y, θ). φ_x and φ_y are very small, so we assume that terms of second or higher orders of φ_x and φ_y are very small and are neglected. The kinetic energy of each component is written as :

$$\begin{aligned} T_{Di} =& 1/2[m_i(\dot{u}^2 + \dot{v}^2 + \dot{w}^2) + I_{Di}(\dot{\theta}^2 + 2\dot{\theta}\dot{\varphi_x}\varphi_y) + I_{Pi}(\dot{\varphi_x}^2 + \dot{\varphi_y}^2) \\ &+ 2m_i.z_i(\dot{\varphi_x}\dot{u} - \dot{\varphi_x}\dot{v} - \dot{\varphi_y}\dot{w}\varphi_y) + 2m_i.z_i^2(\dot{\varphi_x}^2)] \end{aligned} \tag{26}$$

where m_i is the mass of each component of the rotor i.e parts shafts and disks, I_{Di} and I_{Pi} are respectively the diametrical and polar moment of inertia of each component, z_i is the distance of the mass center of each element Gi to the mass center of system Gs. The terms $m_i.z_i$ and $m_i.z_i^2$ are due the fact the rotor is not symmetric. The term $2\dot{\theta}\dot{\varphi}_x\varphi_y$ in the equation (26) represents the gyroscopic effect. The displacement and rotation of the system at its mass center are gathered in $\{X\}$:

$$\{X\} = \{u; v; w; \varphi_x; \varphi_y; \theta\} \tag{27}$$

The application of the Lagrange equations on the kinetic energy of the rotor elements lead to the following matrix form equation:

$$\frac{d}{dt}(\frac{\partial T_D}{\partial \dot{X}}) - (\frac{\partial T_D}{\partial X}) = [M_{cste}] + ([dM\{X\}])\{\ddot{X}\} + \{F_{dyn}\{\dot{X}\}\} + \{F_{coup}\{\dot{X}\}\} \tag{28}$$

M_{cste} is the classical mass matrix, $[dM\{X\}]$ is the terms in the mass matrix that are influenced by $\{X\}$ due to the non-stationary regime assumption, $\{F_{dyn}\{\dot{X}\}\}$ the force vector related to the gyroscopic effect of the elements of the rotor and $\{F_{coup}\{\dot{X}\}\}$ has only a non-nill moment on the degree of freedom of angular deformation which is due the gyroscopic terms included in the model. If the particular case of model with no gyroscopic effect is considered, the contribution of the matrix $\{F_{coup}\{\dot{X}\}\}$ and $\{F_{dyn}\{\dot{X}\}\}$ becomes nill since the term $2\dot{\theta}\dot{\varphi}_x\varphi_y$ in the equation (26) will be equal to zero.

2.5.2 Overall dynamic equation of the rotor

The dynamics model is developed based on the restitution forces and is given by the following equation.

$$[M_{cste}] + ([dM\{Q\}])\{\dot{Q}\} = [F_{ext}] - [F_{dyn}\{Q\}] - [F_{coup}\{Q\}] + [F_{connect}] \tag{29}$$

where

$$\{Q\} = \{\{X\}; \{\dot{X}\}\}; [F_{connect}] = [F_{bearing}\{Q\}] + [F_{gear}\{Q\}] \tag{30}$$

$F_{ext}(t)$ is the external effort and $[F_{connect}\{\mathrm{Q}\}]$ is the forces due to the connecting elements. The connecting elements in our case are the bearings and gears. $F_{bearing}\{Q\}$ is the force vector from the bearing internal forces. $F_{gear}\{Q\}$ is the force vector from the gear contact forces.

3 Numerical Simulation

The preceding developments were applied to run a numerical example of a simple dynamic rotor system with a rigid shaft, and two rigid disks (gears) supported by two ball bearings. The damping and stiffness of the bearings are given by: c = 100 $\mathrm{N\,m^{-1}\,s}$ and k = 5×10^7 $\mathrm{N\,m^{-1}}$. The geometric and material properties of the rotor (shaft, gear, bearing) used in the simulation are reported in tables 1 to 4 in Appendix B. A constant driving torque of 200 $\mathrm{N\,m}$ is introduced to the system. The simulations were run in different conditions for 100 shaft revolutions. For the first analysis, the simulation is run in two different configurations of bearing BPFOs (BPFO = 4.5 and 9) to highlight the differences in the variations in the IAS due to the change in the bearing BPFOs.

Figure 5a shows the response of the "macroscopic" angular speed of the system. For this analysis, we only consider the steady-state part of the run, as we are studying only the excitations from the bearing. So, the first 50 shaft revolutions are neglected as it is in the non-stationary regime and they can have transient effects. It should be reminded that the resistive moment due to the bearings depends on the load applied to the bearing and the fluctuations in this resistant moment depend on the BPFO of each bearing. The Figure 5b clearly shows the angular speed of the system is directly influenced by the BPFO of the bearings, that is the angular frequency of the IAS is the BPFO expressed in the angular domain which is 4.5, and 9 events per revolution for each simulation.

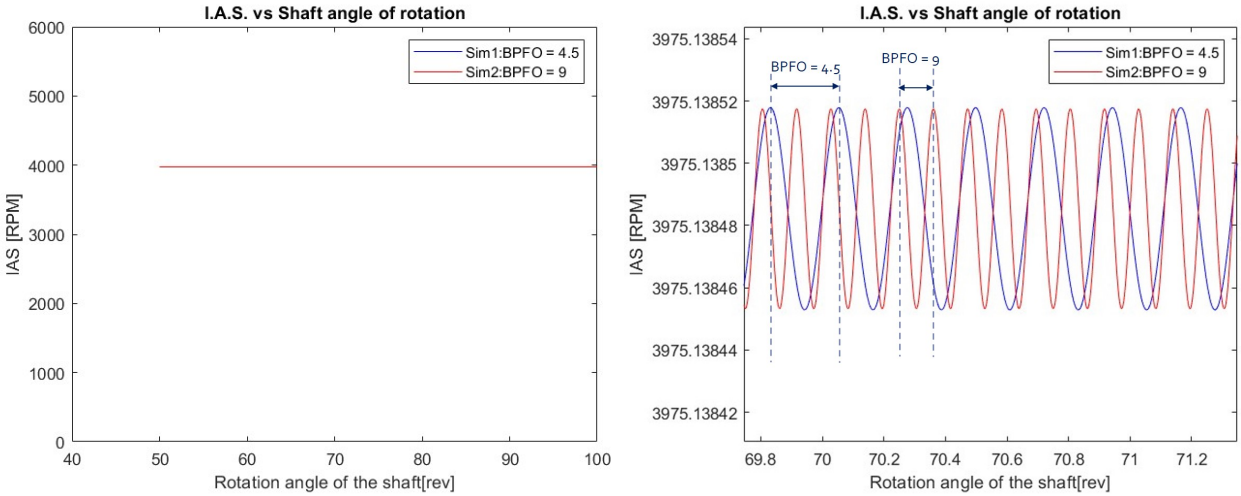

(a) Angular speed of the system

(b) Zoomed view

Figure 5: Angular Speed of the shaft for different bearing BPFO

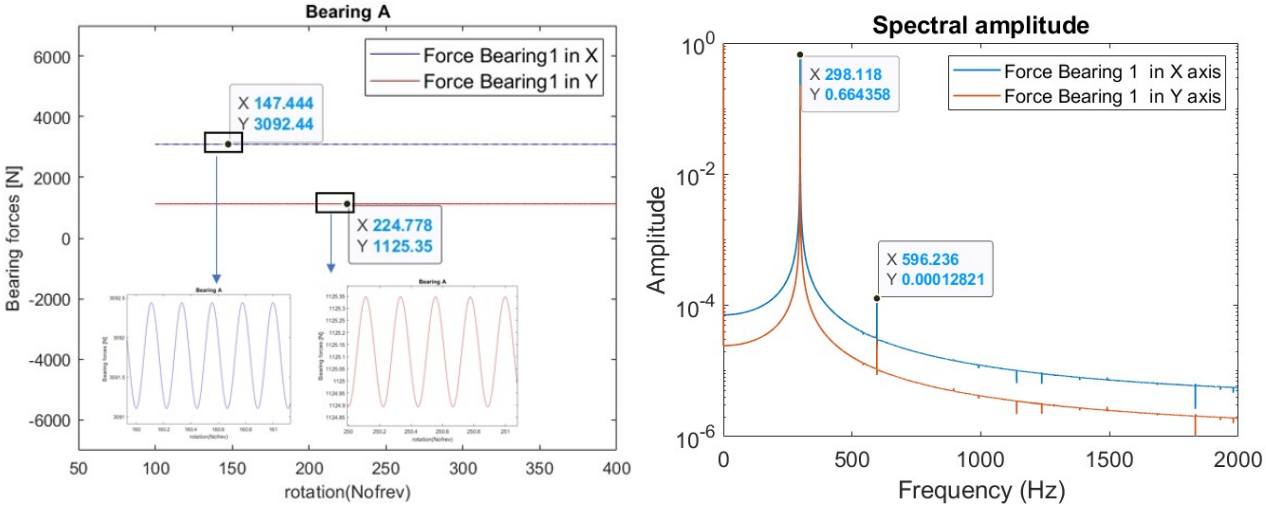

(a) Force Acting on the Bearing A

(b) Frequency response of the forces on the Bearing A

Figure 6: Forces in bearing A for simulation with BPFO= 4.5 and speed at 4000 rpm

This demonstration shows that even when the magnitude of these fluctuations is very low, these can excite other harmonics in the system which the reader must take care of while simulating such systems. So, It is very important to establish there are strong couplings between the rotation of the shaft and forces due to the connecting elements in the model. The graphs in the Figure 6a show the forces acting in bearing A for simulation 1. The fluctuations in the forces in both X and Y directions are due to the harmonic excitations which are dependent on the BPFO of the bearings. Figure 6b shows the spectral response of the forces in the X and Y directions. There are 2 main orders which are visible, 1^{st} peak is at 298 Hz and the 2^{nd} is at 596 Hz, which corresponds to the excitations due to the BPFO of the bearing (which is 4.5 in this case). But it can be seen that there are other smaller excitations with low amplitudes at higher frequencies. This is due to the fact that the rotational speed is not constant (advanced research works are going on regarding these phenomena at LaMCoS). So, even in stationary conditions when the IAS is considered as an unknown of the dynamic problem rather than the assumption of being constant, it can be seen that it highly influences the dynamic behavior of the system.

4 Parametric Study

4.1 Effect of gyroscopic at higher speeds

In order to reach very high speeds, the rotational damping of the system is decreased to C = 0.0307 $\mathrm{N\,m^{-1}\,s}$. The simulation is then run for 300 rotations. To study the effects of gyroscopic influence on the system at very high speeds, the simulation is run in two conditions. In the first condition, the gyroscopic effects are included in the simulation, and in the second condition, the gyroscopic effects are not included. This can be done by neglecting the matrix $\{F_{coup}\{\dot{X}\}\}$ and $\{F_{dyn}\{\dot{X}\}\}$ since the term $2\dot{\theta}\dot{\varphi}_x\varphi_y$ in the equation (26) will be equal to zero. The damping and all other geometric properties are kept the same from the previous simulations. However, to induce more tilting moments due to the gyroscopic effect, the two bearings are set to have different stiffness (see Table 1). A constant driving torque of 200 $\mathrm{N\,m}$ was introduced.

Table 1: Stiffness of the bearings in case 1 and case 2

Bearing Name	K($\mathrm{N\,m^{-1}}$)
Bearing A	5×10^8
Bearing B	1×10^8

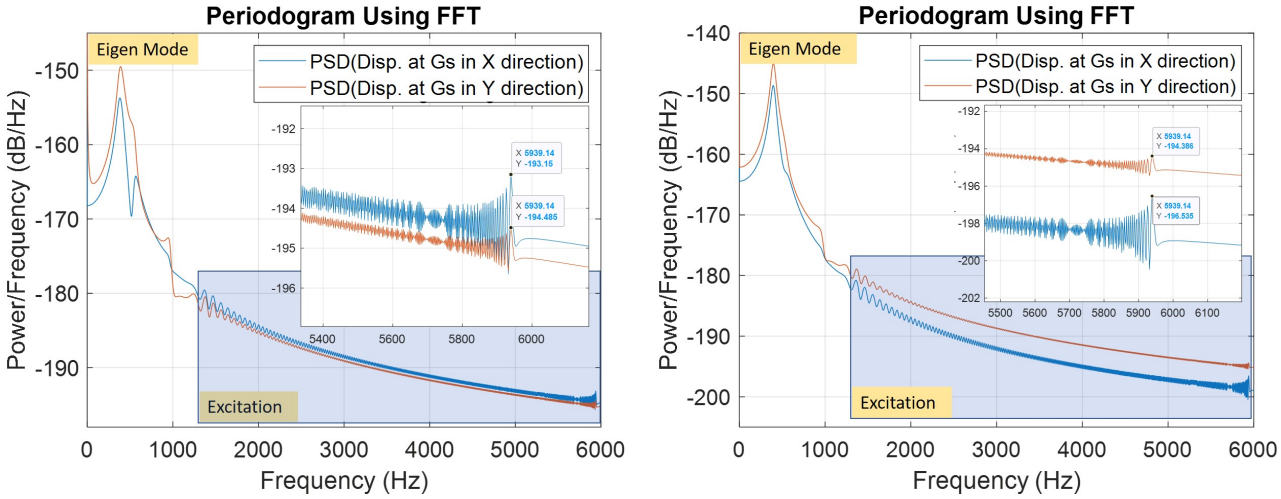

(a) Response with gyroscopic effects

(b) Response without gyroscopic effects

Figure 7: Spectral Response of the system

The graph in the Figure 7a and Figure 7b shows the power spectral density estimates using FFT of displacement in X and Y directions at Gs for both simulations. The system reaches 40000 rpm in both cases. In both cases, the eigenmodes are at 390 Hz and the shapes are a bit different between the two graphs are due to the non-linear effects introduced by gyroscopic coupling. The frequency of the excitation due to the bearing, as it is dependent on the angular speed of the system, increases from around 1200 Hz to 6000 Hz when the speed is increasing. The key differences to note in these graphs are the amplitude in the X direction in gyroscopic and non-gyroscopic cases.The low db is because the obtained displacements are in m. The amplitude in the X direction at the highest speed, for the gyroscopic condition, is 4 dB higher than the amplitude in the X direction for the non-gyroscopic condition (-197 dB in case of non-gyroscopic and -193 dB in case of gyroscopic). But the difference in amplitude in the Y direction in the case of gyroscopic and non-gyroscopic cases is almost negligible. This difference is because the gyroscopic term $2\dot{\theta}\dot{\varphi}_x\varphi_y$, which is dependent in rate of change of rotation in X ($\dot{\varphi}_x$) and only in rotation in Y (φ_y).

This behavior is attributed to the use of Euler angles for the transformation of rotation and its non-symmetric nature of equations. The gyroscopic term introduces an extra term ($I_p\ddot{\theta}\dot{\varphi}_y$) in the equation attributed to φ_x

which is not present in equation attributed to φ_y and the displacements at the bearing in X and Y are dependent on φ_x and φ_y. Further analysis shows that the influence of θ on φ_x and φ_y are more profound, these tilting rotations directly influence the system displacement in X and Y. When the speed of the rotation decreases to 4000rpm, the difference in amplitudes in the X direction between gyroscopic and non-gyroscopic cases was found to be 1 dB. It is very important to note that, the assumptions made by classical approaches, of that given law of the rotational speed can lead to the non-replicability of these phenomena in high-speed conditions. Because by considering IAS as an implicit function of the system, it shows us that it can highly influence the rotor dynamic properties of the system, especially when working in high-speed conditions.

4.2 Effect of gear contact position at higher speeds

The same high-speed condition simulation is run with gyroscopic effects included but in two new cases. In the first case, the gears contact position (ϕ) is 0 degrees, and in the second case, ϕ at 90 degrees, i.e the contact of gears are on $\vec{\tilde{y}}$ and $\vec{\tilde{x}}$ axis respectively. The stiffness of the bearings are given by: k = 5×10^7 $\mathrm{N\,m^{-1}}$, damping, and all other geometric properties are kept the same from the previous simulations. The simulation is then run for 900 rotations. The steady-state part of the simulation is considered for this analysis and the simulation was run with multiple ODE solvers to check for result consistencies and numerical errors.

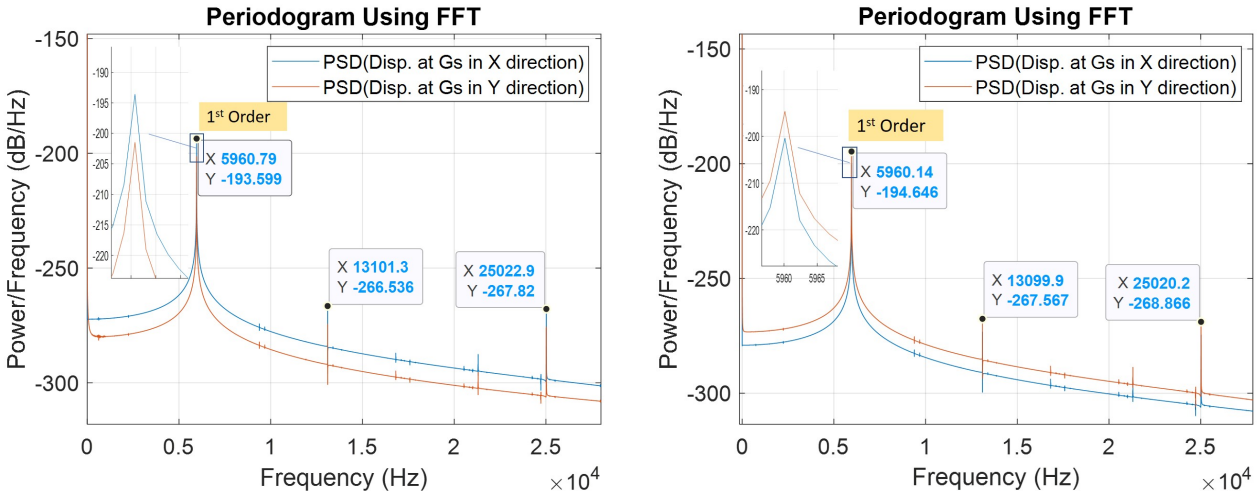

(a) Response at $\phi = 0°$

(b) Response at $\phi = 90°$

Figure 8: Spectral Response of different gear contact position(ϕ)

The graphs in the Figure 8a and Figure 8b shows the power spectral density estimates using FFT of displacement in X and Y directions at Gs for both simulation conditions. The peak frequency amplitude at $\phi = 0°$ shows that the amplitude at X is more than at Y and the peak frequency amplitude at $\phi = 90°$ shows displacement at Y is more than at X. This is obvious because the forces acting on the gear (F_T and F_R) are reversed in X and Y directions as we switch from $\phi = 0°$ to $\phi = 90°$ (F_T is more than F_R). But there are two key differences to be noted in these two cases. The first point to be noted is, The main excitation frequency due to the bearing is at 5961 Hz in the case of $\phi = 0°$ and 5960 Hz in the case of $\phi = 90°$. The peak frequencies for the main excitaions and also other harmonics of the excitation at $\phi = 0°$ is slightly higher than $\phi = 90°$. The second point to be noted is, that the amplitude at peak frequencies at $\phi = 90°$ is slightly higher than $\phi = 0°$ in all excitations by 1 dB/Hz. This is why there is a small decrease in peak frequencies in the case of $\phi = 90°$ compared to $\phi = 0°$. The energy loss due to vibration content for $\phi = 90°$ is more than $\phi = 0°$, so it cannot achieve the same rotational speed as that of $\phi = 0°$. This should not be the case, as the system is symmetric in both the X and Y axis i.e the spring stiffness and damping are the same in the X and Y directions and the only change is the gear forces acting on the system. This behavior is also attributed to the non-symmetric nature of equations when using Euler angles. The gyroscopic term introduces an extra term ($I_p\ddot{\theta}\dot{\varphi}_y$) in the equation attributed to φ_x which is not present in equation attributed to φ_y and the displacements at the bearing in

X and Y are dependent on φ_x and φ_y. So, when the forces acting in the Y direction are more than those acting in X, as in the case of ϕ = 90° (F_T is acting in the Y direction), the displacement and rotations in Y are higher, which leads to the increase in the vibration content due to the term $I_p\ddot{\theta}\dot{\varphi}_y$. This is reason why ϕ = 90° has slightly higher amplitude peak frequencies amplitude when compared to ϕ = 0°. It is also to be noted that this extra term ($I_p\ddot{\theta}\dot{\varphi}_y$) is proportional to the rotational acceleration and does not exist when the speed is constant. Further analysis shows that, when the speed of rotation is further increased to 60000 rpm, the differences in the peak frequency amplitudes increase to 1.2 dB. This shows the influences of rotational speed and why it should be considered as an implicit variable when working with higher speeds.

5 Conclusion

This paper develops a simplistic model of an e-powertrain based on the angular approach, considering no assumption on the IAS. A simplistic novel bearing model was established based on the hypothesis that the rolling resistance phenomenon is occurring due to the interaction between the races and the rolling elements. A harmonic excitation in the bearing was introduced to the system which depends on angular speed and its BPFO. The results show there are small excitations in the response of the system other than the BPFO excitation even in stationary conditions. This is due to the fact the speed of the rotation is not perfectly constant. The other results show that at higher speeds when we introduce gyroscopic couplings in the system, the system's dynamic response is influenced by the speed due to the strong couplings between the rotations in X and Y and the speed. The results from the effects of gear contact location show that there are subtle differences in the peak frequency amplitudes and the peak frequencies when we switch the gear positions from ϕ = 0° to 90°, this is due to the non-symmetric nature of Euler angle transformations that should be accounted for when working with high speeds. Based on the results, we can see that angular speed has a high influence on the dynamics of the system, especially in high-speed conditions. All these results show that suppressing the constant speed assumption may change the model classically used in the literature. This work will be further extended to study the effects of the electric motor on the overall drive line for validating source identification related to its kinematic.

Acknowledgements

This is part of the "ECO DRIVE" project, funded by the European Commission through the H2020 "Marie Skłodowska-Curie Innovative Training Networks" program (grant number 858018) and focusing on noise and vibration in eco-efficient powertrains of future vehicles.

References

[1] G. Darroch. (2017) Netherlands 'will pay the price' for blocking turkish visit – erdoğan. [Online]. Available: http://newsroom.unfccc.int/media/521376/paris-electro-mobility-declaration.pd

[2] F. L. M. dos Santos, J. Anthonis, F. Naclerio, J. J. C. Gyselinck, H. Van der Auweraer, and L. C. S. Góes, "Multiphysics nvh modeling: Simulation of a switched reluctance motor for an electric vehicle," *IEEE Transactions on Industrial Electronics*, vol. 61, no. 1, pp. 469–476, 2014.

[3] C. Martis, D. Fodorean, P. C. Irimia, and C. I. Husar, "Vibroacoustic behaviour analysis of a permanent magnet synchronous machine for automotive applications," in *2014 49th International Universities Power Engineering Conference (UPEC)*, 2014, pp. 1–6.

[4] C. Guangming and X. Yudong, "A statistical model for gears noise prediction in gearbox," in *2010 International Conference on Electrical and Control Engineering*, 2010, pp. 270–272.

[5] M. Åkerblom, "Gearbox noise : Correlation with transmission error and influence of bearing preload," 2008.

[6] D. Kumar, T. Sambharam, S. Kottalgi, P. Mandloi, and O. Kesarkar, "Electric vehicle powertrain multiphysics nvh simulation," in *IECON 2018 - 44th Annual Conference of the IEEE Industrial Electronics Society*, 2018, pp. 490–495.

[7] D. Kumar, S. Kottalgi, T. Sambharam, and P. Mandloi, "A multiphysics optimization approach to design low noise and light weight electric powertrain noise, vibration and harshness (nvh) prediction of electric powertrain using finite element analysis (fea) and optimization," in *IECON 2017 - 43rd Annual Conference of the IEEE Industrial Electronics Society*, 2017, pp. 1692–1697.

[8] Y. Fang and T. Zhang, "Modeling and analysis of electric powertrain NVH under multi-source dynamic excitation," in *SAE Technical Paper Series*. SAE International, Oct. 2014. [Online]. Available: https://doi.org/10.4271/2014-01-2870

[9] P. K. Gupta, "Dynamics of Rolling-Element Bearings—Part III: Ball Bearing Analysis," *Journal of Lubrication Technology*, vol. 101, no. 3, pp. 312–318, 07 1979. [Online]. Available: https://doi.org/10.1115/1.3453363

[10] J. Hung, "Design of the most efficient excitation for a class of electric motor," *IEEE Transactions on Circuits and Systems I: Fundamental Theory and Applications*, vol. 41, no. 4, pp. 341–344, 1994.

[11] S. Baudin, D. Rémond, J. Antoni, and O. Sauvage, "Non-intrusive rattle noise detection in non-stationary conditions by an angle/time cyclostationary approach," *Journal of Sound and Vibration*, vol. 366, pp. 501–513, 2016.

[12] A. Bourdon, H. André, and D. Rémond, "A New way of writing motion equation in rotating machines by translation into the angular domain," in *8th IFToMM International Conference on Rotordynamics, KIST*, Séoul, South Korea, Sep. 2010, p. CDRom. [Online]. Available: https://hal.archives-ouvertes.fr/hal-00504763

[13] S. Harsha, "Nonlinear dynamic analysis of a high-speed rotor supported by rolling element bearings," *Journal of Sound and Vibration*, vol. 290, no. 1, pp. 65–100, 2006. [Online]. Available: https://www.sciencedirect.com/science/article/pii/S0022460X05002233

[14] Q. Han, Y. Chen, H. Zhang, L. Jiang, and X. Li, "Vibrations of rigid rotor systems with misalignment on squirrel cage supports," *Journal of Vibroengineering*, vol. 18, no. 7, pp. 4329–4339, nov 2016. [Online]. Available: https://doi.org/10.21595%2Fjve.2016.16860

[15] J.-C. Luneno, J.-O. Aidanpää, and R. Gustavsson, "Effects of shaft flexibility and gyroscopic coupling on instability threshold speeds of rotor-bearing systems." *13th International Symposium on Transport Phenomena and Dynamics of Rotating Machinery 2010, ISROMAC-13*, 01 2010.

[16] N. Sawalhi and R. Randall, "Simulating gear and bearing interactions in the presence of faults: Part i. the combined gear bearing dynamic model and the simulation of localised bearing faults," *Mechanical Systems and Signal Processing*, vol. 22, no. 8, pp. 1924–1951, 2008. [Online]. Available: https://www.sciencedirect.com/science/article/pii/S0888327007002725

[17] S. Singh, U. G. Köpke, C. Q. Howard, and D. Petersen, "Analyses of contact forces and vibration response for a defective rolling element bearing using an explicit dynamics finite element model," *Journal of Sound and Vibration*, vol. 333, no. 21, pp. 5356–5377, 2014.

[18] X. Hua and E. Gandee, "Vibration and dynamics analysis of electric vehicle drivetrains," *Journal of Low Frequency Noise, Vibration and Active Control*, vol. 40, no. 3, pp. 1241–1251, 2021. [Online]. Available: https://doi.org/10.1177/1461348420979204

[19] J. L. Gomez, I. Khelf, A. Bourdon, H. André, and D. Rémond, "Angular modeling of a rotating machine in non-stationary conditions: Application to monitoring bearing defects of wind turbines with instantaneous angular speed," *Mechanism and Machine Theory*, vol. 136, pp. 27–51, 2019. [Online]. Available: https://www.sciencedirect.com/science/article/pii/S0094114X18315489

[20] P. Arvid, in *LES ROULEMENTS - Description - Théorie - Applications*, 1967, pp. 50–60.

Appendix

A Nomenclature

$BPFO$	Ball Pass frequency outer
F_r	Radial forces acting on the connecting elements
F_t	Tangential forces acting on the connecting elements
F_{bear}	Forces acting on the bearings
T_f	Resistive (frictional) torque acting on the bearings
F_{gear}	Forces acting on the gear
M_{gear}	Moment acting at center of gravity of system(Gs) due to the gear forces

B Numerical Simulation data

The geometric and material properties of the rotor (shaft, gear, bearing, motor) used in the simulation are reported in table 1 to table 4 in Appendix B.

Table 2: Shaft properties

Symbol	Quantity	Value
L	Length of shaft	0.139 m
Do	Outer shaft diameters	0.025 m
Di	Internal shaft diameter	0 m
ρ	Density Gear	7870 $\mathrm{kg/m^2}$
υ	Poisson Ratio	0.3

Table 3: Gear Properties

Symbol	Quantity	Value
M_g	Modulus of the primary gear	1.578
Z_g	No. of teeth on the primary gear	37
h	Thickness of disk	0.02 m
ρ	Density Shaft	7870 $\mathrm{kg/m^2}$
υ	Poisson Ratio	0.3
L_{g1}	Distance of gear 1 center from left end	0.050 m
L_{g2}	Distance of gear 2 center from left end	0.059 m

Table 4: Bearing Properties

Symbol	Quantity	Value
a_{cf}	co-relation factor for force	0.0002
a_f	co-relation factor for torque	0.0001
μ	Frictional gear coefficient	0.015
Do	Outer diameter of the bearings	0.062 m
h	Thickness of disk	0.02 m
L_{b1}	Distance of bearing 1 center from left end	0.016 m
L_{b2}	Distance of bearing 2 center from left end	0.083 m